doi: 10.3978/j.issn.1000-4432.2021.03.02
View this article at: https://dx.doi.org/10.3978/j.issn.1000-4432.2021.03.02

发生于眶骨的占位性病变CT和病理表现及其相关性

王婷婷[1]，刘勋[2]，朱利民[2]，林婷婷[2]，何彦津[2]

(1. 西安市第一医院眼科，陕西省眼科研究所，西安 710002；
2. 天津医科大学眼科医院眼眶病与眼整形科，天津 300384)

[摘　要]　**目的：**分析发生于眶骨的占位性病变的CT表现及其与组织病理学之间的关系。**方法：**回顾性收集15例经临床表现、影像学特征、病理证实为发生于眶骨占位病变患者的临床资料，分析其CT检查、组织病理学切片及其他临床表现。**结果：**在15例患者中，经病理诊断为骨瘤的患者有4例，骨内血管瘤3例，骨样骨瘤和骨化性纤维瘤各2例，嗜酸性肉芽肿3例，尤文肉瘤1例。骨瘤由成熟板层骨构成，对应在CT上呈现为高密度的骨样结节状隆起；骨内血管瘤病理主要表现为骨小梁间的畸形血管，在CT上表现为典型的“栅栏状”“蜂窝状”特征；骨样骨瘤以骨样组织和结缔组织为主，在CT上为类圆形的高密度影，中央为典型的低密度“瘤巢“影，外周为增生的骨密度影；骨化性纤维瘤由增生的纤维组织及骨样组织构成，CT表现为肿瘤表面常有骨壳包绕，病变多呈圆形或椭圆形；嗜酸性肉芽肿主要由大量朗格汉斯细胞组成，对应CT上的软组织肿块影，可伴溶骨性破坏；尤文肉瘤以低分化的小圆细胞为主，CT表现为虫蚀样骨质破坏，破坏的骨组织间有软组织病变。**结论：**发生于眶骨的各类病变有其特有的病理组成，不同的病理组成在CT上表现出相应的影像特征。

[关键词]　眼眶；骨肿瘤；计算机体层成像；病理学

Computed tomography and pathological manifestations of space-occupying lesions of the orbital bone and their relevance

WANG Tingting[1], LIU Xun[2], ZHU Limin[2], LIN Tingting[2], HE Yanjin[2]

*(1. Department of Ophthalmology, First Hospital of Xi'an, Shaanxi Ophthalmological Institute, Xi'an 710002;
2. Department of Orbital Disease and Oculoplastic Surgery, Tianjin Medical University Eye Hospital, Tianjin 300384, China)*

Abstract　**Objective:** To analyze computed tomography (CT) manifestations of space-occupying lesions of the orbital bone and their relationship with histopathology. **Methods:** The clinical data of 15 patients with orbital bone occupying lesions confirmed by clinical manifestations , imaging features and pathological symptoms features were

收稿日期 (Date of reception)：2020–11–20
通信作者 (Corresponding author)：林婷婷，Email: ltt6123@126.com
基金项目 (Foundation item)：天津市临床重点学科建设项目 (TJLCZDXK7006)。This work was supported by Tianjin Clinical Key Discipline Construction Project, China (TJLCZDXK7006).

retrospectively collected, and their CT examination, histopathological sections and other clinical manifestations were analyzed. **Results:** Among the 15 patients, 4 cases were pathologically diagnosed with osteoma, 3 cases of intraosseous hemangioma, 2 cases of osteoid osteoma and 2 cases of ossifying fibroma, 3 cases of eosinophilic granuloma and 1 case of Ewing's sarcoma. Osteoma was composed of mature lamellar bones, which corresponded to a high-density osteoid nodular protuberance on CT. The pathological features of intraosseous hemangioma were mainly malformed blood vessels between bone trabeculae and typical "fence" and "honeycomb" features on CT. Osteoid osteoma was mainly composed of bone-like tissue and connective tissue, mainly showing round high-density shadow, typical low-density "tumor nest" shadow in the center, and hypertrophic bone density shadow in the periphery. Ossifying fibroma was composed of proliferative fibrous tissue and bone-like tissue. CT showed that the surface of the tumor was often surrounded by bone shell, and the lesions were mostly round or oval. Eosinophilic granuloma was mainly composed of a large number of Langerhans cells, which corresponded to the soft tissue mass on CT and could be accompanied by osteolytic destruction. Ewing's sarcoma was mainly composed of poorly differentiated small round cells, and CT manifestations were worm-eaten bone destruction with soft tissue lesions between destroyed bone tissues. **Conclusion:** Various lesions occurring in the orbital bone have their own special pathological composition. Different pathological components show corresponding imaging features on CT.

Keywords orbit; bone tumor; computer tomography; pathology

发生于眼眶的肿瘤种类繁多且发病率高，发生于眼眶骨的肿瘤或瘤样病变却很少见，据报道眶骨的原发性肿瘤约占眼眶所有肿瘤的0.6%~2.0%[1]。为探讨发生于眶骨的占位性病变临床表现及其CT和病理特征，本研究收集了天津医科大学眼科医院2009年3月至2019年6月共15例经临床表现、影像学特征和病理确诊的原发于眶骨的肿瘤患者，排除了累及多个骨的骨纤维异常增生症和病变继发性侵及眶骨的脑膜瘤、动脉瘤样骨囊肿、神经纤维瘤及各种眶骨的转移癌等。本文主要通过对6种肿瘤[骨瘤(osteoma)、骨内血管瘤(intraosseous hemangioma)、骨样骨瘤(osteoid osteoma)、骨化性纤维瘤(ossifying fibroma)、嗜酸性肉芽肿(eosinophilic granuloma)、尤文肉瘤(Ewing sarcoma)]的临床表现、影像学检查特征的总结以便能提高对该类疾病的认识以及对诊断及其治疗提供一定的帮助。

1 对象与与方法

1.1 对象

回顾性收集天津医科大学眼科医院2009年3月至2019年6月共15例眶骨原发性肿瘤患者的资料，其中男10例，女5例；年龄4.00~54.00(平均27.00)岁；经病理诊断为骨瘤的患者有4例，骨内血管瘤3例，骨样骨瘤和骨化性纤维瘤各2例，嗜酸性肉芽肿3例、尤文肉瘤1例，均为单眼发病。

1.2 方法

常规眼科检查：国际标准视力表检查视力，Hertel眼球突出计行眼球突出度检查。15例患者术前均进行CT检查，术后肿物皆进行组织病理学检查。

1.3 随访

主要通过门诊复查和电话的方式对患者进行随访。包括询问患者有无眼球运动障碍、视力下降、眶周肿物等症状；门诊主要通过影像学检查及眼部查体等方式。

2 结果

2.1 临床表现

裸眼视力0.1~0.5者7例，0.5~1.0者7例，<0.1者1例；眼球突出2只眼相等者5例，2只眼相差1~2 mm者2例，2只眼相差3~5 mm者8例；眼球移位4例，

发现眶周肿物5例，有眼睑及眶周皮肤肿胀者6例，伴视力下降2例，无症状者1例，眼球运动受限4例。

2.2 预后

对患者进行0.5~9.0年的随访，其中1例骨样骨瘤患者术后2次复发，尤文肉瘤患者术后予以放疗和化疗，随访1年无复发；余患者皆未见复发。

2.3 CT表现及病理结果

对骨瘤(图1)、骨内血管瘤(图2)、骨样骨瘤(图3)、骨化性纤维瘤(图4)、嗜酸性肉芽肿(图5)、尤文肉瘤(图6)进行分析，发现在发病部位、病理组成及影像学表现方面有各自的特点，详见表1。

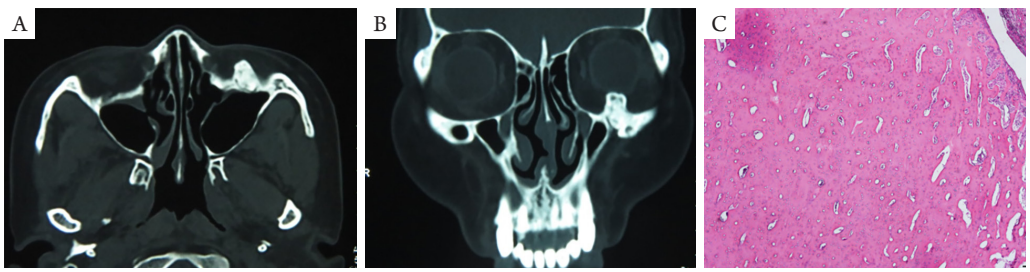

图1 骨瘤眼眶CT图像和病理学表现

Figure 1 CT images and pathological findings of orbital osteoma

(A)水平位CT示左眶下壁密度增高骨硬化影像，密度均匀，有明显边缘，肿瘤边缘规则，无溶解破坏；(B)冠状位CT示眶下壁骨样密度影，向眶内突出挤压眼球；(C)镜下见少量纤维结缔组织和骨小梁组成(HE，×5)。

(A) Horizontal CT showed the increased density of the left inferior orbital wall with uniform density and obvious edge. The edge of the tumor was regular, without dissolution and destruction; (B) Coronal CT showed high-density shadow of the infraorbital wall, protruding into the orbit and squeezing the eyeball; (C) A small amount of fibrous connective tissue and bone trabeculae were seen under the microscope (HE, ×5).

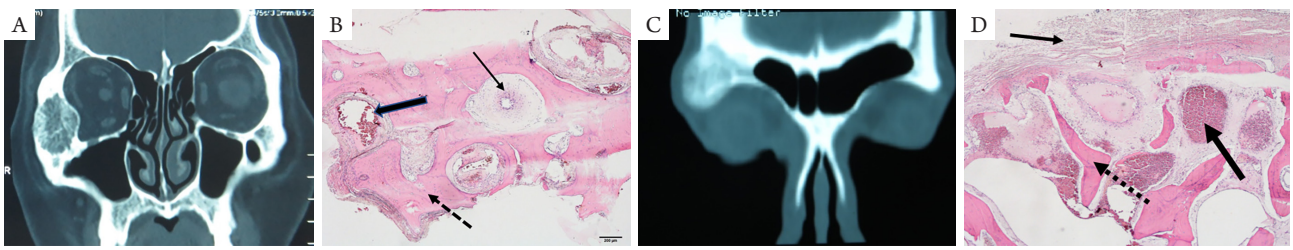

图2 骨内血管瘤CT图像和病理学表现

Figure 2 CT images and pathological findings of intraosseous hemangioma

(A)例1患者CT图像：右侧颧骨膨胀性生长肿物影，呈栅栏状、蜂窝状混杂密度影，内密度不均，可见粗大骨嵴影；(B)例1患者病理结果，骨小梁(虚线箭头)间可见管腔大小不等的血管结构(粗、细箭头)；(C)例2患者CT图像：右侧眶骨肿物，内高低密度混杂；(D)例2患者病理：细箭头指向骨膜，虚线箭头指向骨样基质，粗箭头指向位于骨小梁间的海绵状血管瘤结构(HE，×5)。

(A) CT image of patient 1: The swelling growth tumor shadow of the right cheekbone is palisade like and honeycomb like mixed density shadow. The internal density is uneven, and thick bone ridge shadow can be seen; (B) Pathological results of patient 1: Vascular structures (thick and thin arrows) with different lumen sizes can be seen between trabeculae (dotted arrows); (C) CT image of patient 2: right orbital bone mass, mixed high and low density; (D) Pathological results of case 2: The thin arrow points to periosteum; the dotted arrow points to osteoid matrix, and the thick arrow points to the spongy cavernous hemangioma structure between trabeculae (HE, ×5).

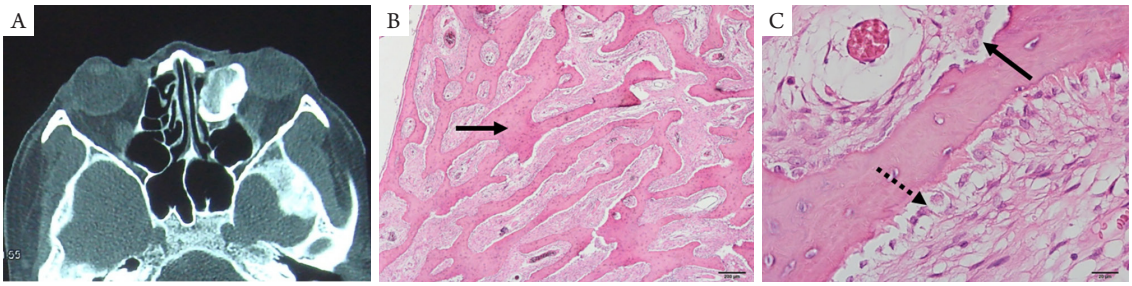

图3 骨样骨瘤眼眶CT图像和病理学表现

Figure 3 CT images and pathological findings with the orbit of osteoid osteoma

(A)左侧筛窦团块状混杂密度影，致密的硬化骨皮质包绕1个可透射线的“瘤巢”，向左眶内生长，左眶内壁骨质不连续。外周为密度增高的骨硬化影像，密度均匀，有明显边缘，无溶解破坏；(B)病理示肿瘤组织为骨细胞及骨样基质所构成，含有纤维组织及骨样骨小梁，箭头指向骨小梁(HE，×5)；(C)实线箭头指向破骨细胞，虚线箭头指向成骨细胞(HE，×40)。

(A) Mass mixed density shadow in the left ethmoid sinus mass, dense sclerotic bone cortex surrounding a radiolucent "tumor nest", and growing in the left orbit, with bone discontinuity in the left orbital wall. Peripheral bone sclerosis images with increased density, uniform density, obvious edge, no dissolution, and no destruction; (B) Pathological results showed that the tumor tissue was composed of bone cells and osteoid matrix, containing fibrous tissue and osteoid trabeculae. The arrow points to trabeculae (HE, ×5); (C) The solid line arrow points to osteoclasts and the dotted arrow points to osteoblasts (HE, ×40).

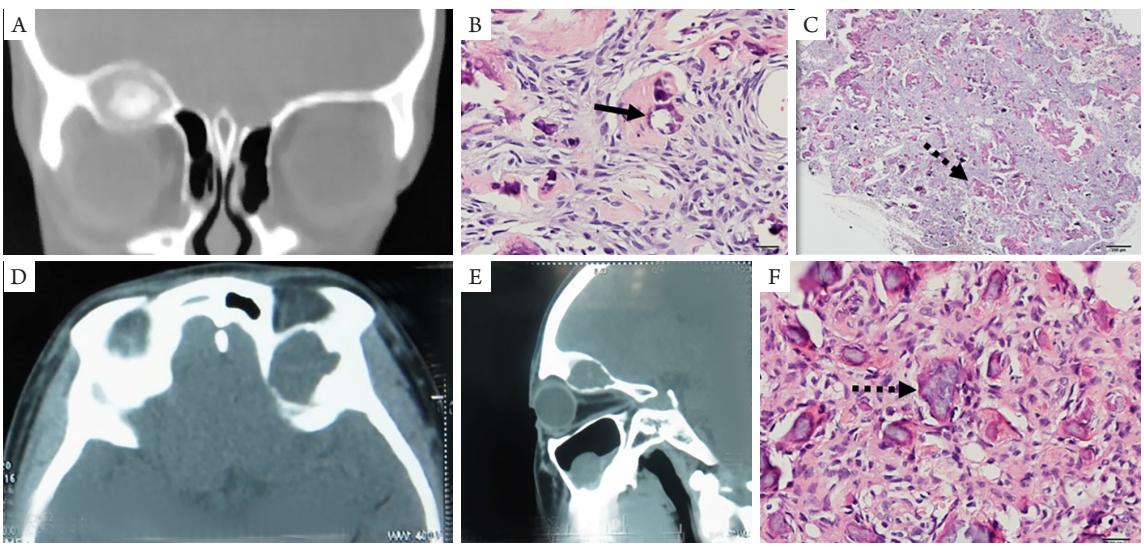

图4 骨化纤维瘤眼眶CT图像和病理学表现

Figure 4 CT images and pathological results of ossifying fibroma

(A~C)患者1，男，6岁：(A)冠状CT示右眶上壁骨质膨隆，内含低密度软组织区，中央含有边界不清的毛玻璃样骨密度影。眼球受压突出并向下移位；(B)纤维组织中含有骨小梁(虚线箭头；HE，×5)；(C)中骨小梁可表现为不规则的矿化(实线箭头；HE，×40)。(D~F)患者2，女，22岁：(D)水平CT示左眶上壁骨质膨隆，内含软组织密度占位病变；(E)矢状位CT示眶上壁骨质膨隆，外周高密度内含软组织密度占位病变；(F)病理示成纤维性间质内含骨小体结构(虚线箭头；HE，×40)。

(A–C) Patient 1, male, 6 years old: (A) Coronal CT shows bone swelling in the right superior orbital wall, including low-density soft tissue area, with ill-defined ground-glass opacity of bones in the center. The eyeball is compressed and displaced downward; (B) Bone trabeculae in fibrous tissue (dotted arrow) (HE, ×5); (C) The trabecular bone shows irregular mineralization (solid arrow) (HE, ×40). (D–F) Patient 2, female, 22 years old: (D) Horizontal CT shows left supraorbital bone swelling, including soft tissue density occupying lesions; (E) Sagittal CT showed that the supraorbital wall was swollen with peripheral high density and soft tissue density occupying lesions; (F) Pathological results showed that fibrous stroma contained bone corpuscles (dotted arrow) (HE, ×40).

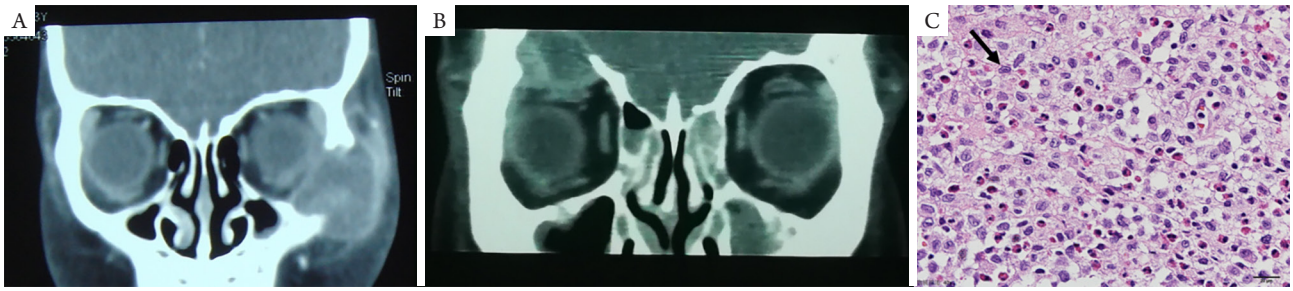

图5 嗜酸性肉芽肿眼眶CT图像和病理学表现

Figure 5 CT image and pathological findings of the orbit with eosinophilic granuloma

(A)患者1，冠状位CT示左侧眶骨内可见形状不规则，边界清楚的肿物，呈中高密度不均质的软组织肿块，肿块内有骨成分，与骨壁缺损关系密切；(B)患者2，冠状位CT示右额骨内形状不规则，边界清楚的肿物，不均质的中高密度软组织肿块，肿块内有高密度影；(C)镜下可见大量朗格汉斯细胞(实线箭头)，伴弥漫分布的嗜酸性粒细胞及少量小淋巴细胞浸润(HE，×40)。

(A) Patient 1: Coronal CT shows irregular shape and well-defined mass in the left orbital bone, showing heterogeneous medium and high-density soft tissue mass with bone components, which are closely related to bone wall defect; (B) Patient 2: Coronal CT shows irregular, well-defined mass in the right frontal bone, heterogeneous medium and high-density soft tissue mass with high-density shadow in the mass; (C) A large number of Langerhans cells can be seen (solid arrow) with diffuse eosinophils and a small number of small lymphocytes infiltration (HE, × 40).

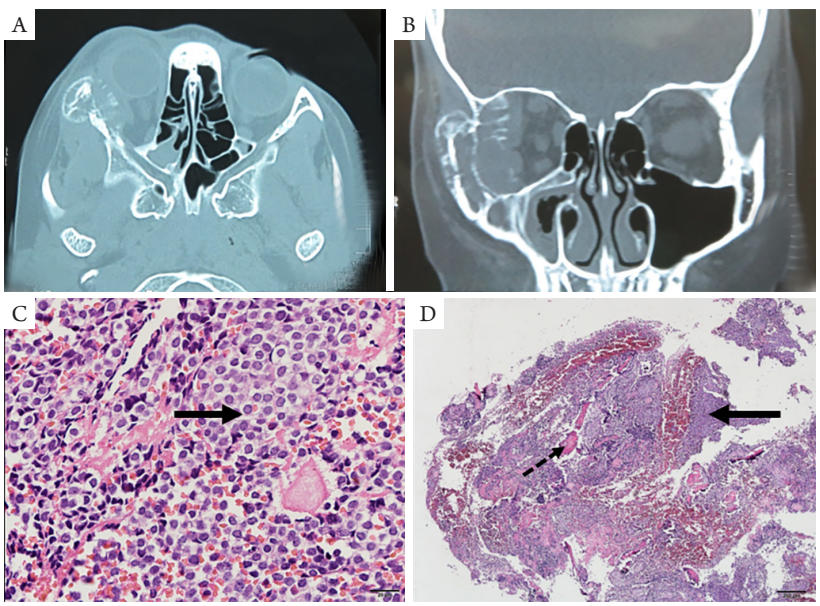

图6 尤文肉瘤眼眶CT图像和病理学表现

Figure 6 CT images and pathological findings of Ewing's sarcoma

(A)水平位CT示右侧上颌骨颧突部骨质溶解破坏，病变向后累及蝶骨大翼；(B)冠状位CT示病变向上累及额骨，向下延伸至上颌窦壁，内有放射状骨针形成。肿瘤穿破骨皮质形成软组织密度肿块，向眶内膨隆推挤眼球及眶内组织向内侧移位。(C，D)病理见小圆细胞肿瘤(实线箭头)核圆形，染色质细腻，可见小核仁(HE，×40)；(D)肿瘤细胞间可见骨小梁(虚线箭头；HE，×5)。

(A) Horizontal CT showed osteolysis and destruction of the zygomatic process of the right maxilla, and the lesion involved the great wing of sphenoid bone backward; (B) Coronal CT showed that the lesion extended upward to the frontal bone and downward to the wall of maxillary sinus, with radial bone needle formation. The tumor penetrated through the bone cortex to form a soft tissue density mass, which bulged into the orbit and pushed the eyeball and orbital tissue to the medial side; (C, D) Small round cell tumor (solid arrow) with round nucleus, fine chromatin, and small nucleoli (HE, × 40); (D) Bone trabeculae between tumor cells (dotted arrow) (HE, × 5).

表1 发生于眶骨的占位性病变影像及病理结果

Table 1 Imaging and pathological results of space occupying lesions in orbital bone

类型	病变部位	CT表现	病理表现
骨瘤	额骨2例，上颌骨1例，额窦眼眶同时受累1例	边界清楚，形状规则，密度均匀的高密度影	由少量纤维结缔组织和不规则致密的骨小梁组成
骨内血管瘤	颧骨2例，额骨1例	典型的“栅栏状”“蜂窝状”或“囊状”骨小梁结构，肿瘤可表现为不同密度影	骨小梁间血管增生，有血窦和动静脉血管畸形区
骨样骨瘤	颧骨1例，筛窦侵及眼眶1例	类圆形的高密度影，中心可见典型的低密度伴钙化的“瘤巢”影，外周伴骨质增生	由骨细胞及骨样基质所构成，含有纤维组织及骨小梁，骨小梁旁可有成骨细胞、破骨细胞
骨化性纤维瘤	额骨2例	肿瘤表面常有骨壳包绕，边界清楚，中央可表现为含有边界不清的毛玻璃样骨密度影或软组织密度占位病变	纤维组织中含有骨小梁，骨小梁表面有成骨细胞；或成纤维性间质内含类似骨小体的小骨块
嗜酸性肉芽肿	额骨1例，颧骨2例	软组织肿块影，不规则、锯齿状的溶骨性破坏	大量朗格汉斯细胞，伴弥漫分布的嗜酸性粒细胞及少量小淋巴细胞浸润
尤文肉瘤	颧骨1例	软组织低密度影，虫蚀状骨质破坏，肿物内有放射状骨针	小圆细胞肿瘤，核圆形，染色质细腻，可见小核仁，核分裂象多、异型性明显

3 讨论

发生于眼眶骨的肿瘤发病率较低，临床少见。由于眼眶骨与眼球等眶内容物关系密切，所以眶骨的肿瘤病变大多以眼球位置及运动改变、视力变化、眶周肿物等症状就诊，若为恶性肿瘤则还可能伴有全身转移的相应表现。在一些起病隐匿的骨肿瘤中，初期也可能并无体征和表现，大多为偶然发现或当肿瘤发展到一定的程度，累及周围组织时才会出现相应的临床症状。

骨瘤，又名骨细胞瘤，是一种比较常见的骨源性良性肿瘤，肿瘤被分为象牙型、成熟型和混合型3种类型。好发于额窦和筛窦，偶见于眶壁骨骼，一般无明显的症状，当肿瘤增长蔓延至眶内时可出现眼球运动障碍、斜视和眼球突出等症状。肿瘤可向骨表面和髓腔生长，可突入窦腔、眼眶，使颅面畸形，骨瘤增大极缓慢[2-3]。病理见瘤体主要由异常排列的成熟板层骨组成，因此大量的骨成分使肿瘤在CT上一般表现为骨表面边界清楚，形状规则，密度均匀的高密度影，与眶骨显影类似。

骨内血管瘤是一种骨内血管畸形，部分患者伴有局部外伤史；肿瘤分为海绵状血管瘤、毛细血管瘤和混合型3种类型[4]。海绵状血管瘤主要由扩大的血性窦腔构成，毛细血管瘤为增生扩张的毛细血管构成。肿瘤位于骨小梁之间，因此在CT上主要表现为密度较低的肿物间有放射状高密度的骨小梁结构，呈现出典型的“栅栏状”“蜂窝状”[5]。偶也可表现为囊状结构，可能是当肿瘤较大时压迫骨小梁导致其破坏和吸收而形成。在本组病例中，病例1的CT表现密度较低，有典型的“栅栏状”状结构，术中出血较多，术后病理结果显示肿瘤中有管腔大小不等的血管样结构；病例2的CT显示为不均匀的较高密度影，术中出血较少，术后病理示血管组织主要为薄壁血管或血窦。因此，我们可以通过影像表现对组织成分有一定的了解，对于在CT上表现为密度较低且有典型的“栅栏状”结构的一类肿瘤，可能血管成分含量相对较多，因此术中较易出血；而对于密度较高的一类肿瘤，组成的血管成分主要为血窦，术中不易出血。

骨样骨瘤是以骨样组织和结缔组织构成“瘤

巢”为主要特征的良性肿瘤。肿瘤可发生在骨骼的各个部位，多见于长骨，眼眶少见，具有有限的生长潜能，术后肿瘤较易复发。“瘤巢”周围可伴有不同程度的骨质增生、硬化[6-7]。大多患者都有疼痛的表现，疼痛会因病情进展而逐渐加重且持续。这种疼痛可能是因为病灶内产生前列腺素而引起，因此服用水杨酸类药物可能对疼痛有一定的缓解作用，但对疾病进展无控制作用[8-9]。成骨细胞和纤维结缔组织可构成骨样骨瘤的特征性“瘤巢”结构，在CT上表现为低密度团块影，病变中伴有的钙化和外周增生的骨质呈高密度影；但有时周围的骨质广泛增生时可能不能见到“瘤巢”的特征性表现。

骨化性纤维瘤是一类由增生的纤维组织及骨样组织构成的良性肿瘤，目前认为其骨样结构是在纤维组织基础上形成的[10]；其组织学主要来源于牙周韧带和骨膜或小梁旁未分化的间叶细胞，于上颌骨、额骨和筛骨较多见[11-12]。2006年WHO头颈部肿瘤分类标准[13]将其分为经典型骨化性纤维瘤(ossifying fibroma，OF)、青少年小梁状骨化纤维瘤(juvenile trabecular ossifying fibroma，JTOF)和青少年沙瘤样骨化纤维瘤(juvenile psammomatoid ossifying fibroma，JPOF)3种类型。JTOF的发病年龄为8.5~12.0岁，CT表现为低密度软组织肿物，中央含有边界不清的毛玻璃样骨密度影；镜下增生的纤维组织中以骨小梁为主，骨小梁表面有成骨细胞，该特点可将JTOF与骨纤维异常增殖症区别开，骨纤维异常增殖症主要表现为正常骨结构被纤维组织代替，使骨小梁破坏，排列不规则分布不均匀，CT也常显示缺乏清晰的边界。JPOF的发病年龄约为20岁，病理表现为肿物内含有较多成纤维细胞，肿物组织中可见散在的骨小体结构[14]；CT主要表现为软组织密度占位病变，外周伴有骨质增生，呈典型的“蛋壳样”结构[15]，该特征应与骨样骨瘤相鉴别。在本研究中，1例患者，男，6岁，影像学和病理学符合青少年小梁状骨化纤维瘤的特征；另1例患者，女，22岁，符合青少年砂瘤样骨化性纤维瘤的特征。该肿瘤应与动脉瘤样骨囊肿相鉴别，动脉瘤样骨囊肿主要由扩张的血窦组成，内含血液或血样液体；CT显示肿瘤外周有骨壳包绕，内含由骨脊分隔的空腔，多可见液-液平面。

嗜酸性肉芽肿是朗格汉斯细胞增生症的一种类型，另外2种类型分别为伴全身多器官广泛受累的勒-雪氏病和伴有典型的尿崩症、突眼和骨破坏等表现的韩-薛氏病。根据2016年WHO造血与淋巴组织肿瘤分类[16]，嗜酸性肉芽肿编码为9751/1，属于交界性或不确定性肿瘤。该病多见于小孩，也可发生于年龄较大的患者，多发生于颞上方眶骨边缘，常表现为溶骨性病变，破坏相邻的皮质骨。对于其发生机制尚不清楚，文献[17]指出其原因可能与自身免疫性疾病有关，也可能是因为骨髓多功能干细胞向朗格汉斯细胞转变的过程失控。病变内主要有大量朗格汉斯细胞，伴弥漫分布的嗜酸性粒细胞及少量小淋巴细胞浸润。因此大量的细胞成分在CT上主要表现为软组织肿块影，但当病变尚未穿破骨皮质或肉芽组织被吸收后也可能见不到软组织肿块；眶骨可见不规则、锯齿状的溶骨性破坏。

尤文肉瘤一般好发于青少年，5岁以上男性儿童较多见，肿瘤发生于髓腔，外侵扩展。肿瘤可发生于全身骨骼，多累计四肢长骨骨干，扁骨以髂骨、肋骨多见，而其他骨很少见[18-19]。肿瘤血管丰富、易出血、坏死，形成囊性。肿瘤增大可穿透骨皮质，该肿瘤一般进展较快，很快会发生远处转移，常见转移至骨和肺。尤文肉瘤为小圆细胞的低分化的恶性肿瘤，镜下主要见大量的小圆细胞，可侵犯骨，故影像学检查CT主要表现为软组织低密度肿块影，周围伴虫蚀状骨质破坏，破坏区内残余骨组织呈放射状排列。

发生于眶骨的肿瘤种类较多，影像学表现复杂易混淆，且易引起严重的并发症。因此，尽早发现病变并及时治疗尤为重要；而影像学检查又是相对简单且安全的检查手段，所以能够掌握常见眶骨肿瘤的影像学特征是极其重要的。同时，明确病理诊断对肿瘤后续治疗也有指导作用。将影像学表现与病理学形态对照分析，阐述二者之间的关系，术前对疾病做出评估可以有效减少术中并发症，且对手术范围及术后进一步治疗有一定的指导作用，可提高疾病的诊断与治疗水平。但由于手术一般较复杂，术中分块取出的肿物标本难以完整保留，无法得到其完整的病理学形态。因此，以后应在保证手术成功的基础上尽可能完整取出肿物组织，且对肿物做好标记定位，以便更好地对照分析病理学形态和影像学表现。

开放获取声明

参考文献

1. Selva D, White VA, O'Connell JX, et al. Primary bone tumors of the orbit[J]. Surv Ophthalmol, 2004, 49(3): 328-342.
2. Mchugh JB, Mukherji SK, Lucas DR. Sino-orbital osteoma: a clinicopathologic study of 45 surgically treated cases with emphasis on tumors with osteoblastoma-like features[J]. Arch Pathol Lab Med, 2009, 133(10): 1587-1593.
3. Soni S, Bhargava A. Revisiting peripheral osteoma of the mandible with case series and review of literature[J]. Indian J Otolaryngol Head Neck Surg, 2014, 66(2):212.
4. 丁宜, Bui Marilyn, 孙晶,等. 单中心107例骨原发血管源性肿瘤临床病理分析[J]. 临床与实验病理学杂志, 2016, 32(7): 766-769.
DING Yi, BUI Marilyn, SUN Jin, et al. Primary vascular tumors of bone: clinicopathologic analysis of 107 patients from single center institution[J]. Chinese Journal of Clinical and Experimental Pathology, 2016, 32(7): 766-769.
5. Brandner JS, Rawal YB, Kim LJ, et al. Intraosseous hemangioma of the frontal bone. Report of a case and review of the literature[J]. J Oral Maxillofac Surg, 2017, 76(4): 799-805.
6. Kashkouli MB, Khalatbari MR, Yahyavi T, et al. Primary endo-orbital osteoid osteoma[J]. Orbit, 2008, 27(3): 211-213.
7. Kashkouli MB, Khalatbari MR, Yahyavi T, et al. Primary endo-orbital osteoid osteoma[J]. Orbit, 2008, 27(3): 211-213.
8. Deferm JT, Sca S, Vriens D, et al. Chronic temporomandibular joint pain: two cases of osteoid osteoma and a review of the literature[J]. Int J Oral Maxillofac Surg, 2017, 46(9): 1130-1137.
9. The usefulness of chemical-shift magnetic resonance imaging for the evaluation of osteoid osteoma[J]. Radiologia Brasileira, 2018, 51(3):156-161.
10. Figueiredo LM, de Oliveira TF, Paraguassú GM, et al. Psammomatoid juvenile ossifying fibroma: case study and a review[J]. Oral Maxillofac Surg, 2014, 18(1): 87-93.
11. Khanna M, Buddhavarapu SR, Hussain SA, et al. Cemento-ossifying fibroma of paranasal sinus presenting acutely as orbital cellulitis[J]. J Radiol Case Rep, 2009, 3(4): 18-25.
12. 杨秀萍, 龚树生. 8例青少年鼻窦骨化性纤维瘤的临床病理观察[J]. 中国临床医学, 2003, 10(5): 693-694.
YANG Xiuping, GONG Shusheng. Clinicopathologic observation of the juvenile ossifying fibromas of paranasal sinuses in 8 cases[J]. Clinical Medical Journal of China, 2003, 10(5): 693-694.
13. Barnes L, Eveson JW, Reichart P, et al. Pathology and genetics of head and neck tumors[M]. Geneva: WHO Press, 2006.
14. Kawaguchi M, Kato H, Miyazaki T, et al. CT and MR imaging characteristics of histological subtypes of head and neck ossifying fibroma[J]. Dentomaxillofac Radiol, 2018, 47(6): 20180085.
15. 李学锋, 戴芳, 赵玺龙, 等. 青少年沙瘤样骨化纤维瘤临床病理分析[J]. 临床与实验病理学杂志, 2011, 27(8): 888-890.
LI Xuefeng, DAI Fang, ZHAO Xilong, et al. Clinicopathological analysis of juvenile psammomatoid ossifying fibroma[J]. Chinese Journal of Clinical and Experimental Pathology, 2011, 27(8):888-890.
16. 段瑞. WHO造血与淋巴组织肿瘤分类(2016)[J]. 诊断病理学杂志, 2017, 24(12): 956-958.
DUAN Rui. WHO classification of hematopoietic and lymphoid tumors (2016)[J]. Chinese Journal of Diagnostic Pathology, 2017, 24(12): 956-958.
17. Kitsoulis PV, Paraskevas G, Vrettakos A, et al. A case of eosinophilic granuloma of the skull in an adult man: a case report[J]. Cases J, 2009, 2(1): 9144.
18. 李振武, 李天云, 解非, 等. 尤文肉瘤的影像学诊断[J]. 现代肿瘤医学, 2015(23): 3474-3477.
LI Zhenwu, LI Tianyun, XIE Fei, et al. Value of imaging in the diagnosis of Ewing's sarcoma[J]. Journal of Modern Oncology, 2015(23): 3474-3477.
19. Somarouthu BS, Shinagare AB, Rosenthal MH, et al. Multimodality imaging features, metastatic pattern and clinical outcome in adult extra skeletal Ewing sarcoma: experience in 26 patients[J]. Br J Radiol, 2014, 87(1038): 20140123.

本文引用：王婷婷, 刘勋, 朱利民, 林婷婷, 何彦津. 发生于眶骨的占位性病变CT和病理表现及其相关性[J]. 眼科学报, 2021, 36(9): 719-726. doi: 10.3978/j.issn.1000-4432.2021.03.02
Cite this article as: WANG Tingting, LIU Xun, ZHU Limin, LIN Tingting, HE Yanjin. Computed tomography and pathological manifestations of space-occupying lesions of the orbital bone and their relevance[J]. Yan Ke Xue Bao, 2021, 36(9): 719-726. doi: 10.3978/j.issn.1000-4432.2021.03.02